1 **Chromatography related performance of the Monitor for Aerosols and Gases in Ambient**
2 **Air (MARGA): laboratory and field based evaluation**

3 Xi Chen, John T. Walker[*] and Chris Geron

4 National Risk Management Research Laboratory, Office of Research and Development, U.S.
5 Environmental Protection Agency, Research Triangle Park, North Carolina, 27711, U.S.A.
6 [*]Corresponding Author: Tel.:+1 919 541 2288. Email:Walker.JohnT@epa.gov.

7

8 **Abstract**

9   Evaluation of the semi-continuous Monitor for Aerosols and Gases in Ambient Air
10 (MARGA, Metrohm Applikon B.V.) was conducted with an emphasis on examination of
11 accuracy and precision associated with processing of chromatograms. Using laboratory standards
12 and atmospheric measurements, analytical accuracy, precision, and method detection limits
13 derived using the commercial MARGA software were compared to an alternative
14 chromatography procedure consisting of a custom Java script to reformat raw MARGA
15 conductivity data and Chromeleon (Thermo Scientific Dionex) software for peak integration.
16 Our analysis revealed issues with accuracy and precision resulting from misidentification and
17 misintegration of chromatograph peaks by the MARGA automated software as well as a
18 systematic bias at low concentrations for anions. Reprocessing and calibration of raw MARGA
19 data using the alternative chromatography method lowered method detection limits and reduced
20 variability (precision) between parallel sampler boxes. Instrument performance was further
21 evaluated during a one-month intensive field campaign in the fall of 2014, including analysis of
22 diurnal patterns of gaseous and particulate water soluble species (NH_3, SO_2, HNO_3, NH_4^+, SO_4^{2-}
23 and NO_3^-), gas-to-particle partitioning, and particle neutralization state. At ambient
24 concentrations below ~ 1 $\mu g/m^3$, concentrations determined using the MARGA software are
25 biased +30% and +10% for NO_3^- and SO_4^{2-}, respectively, compared to concentrations determined
26 using the alternative chromatography procedure. Differences between the two methods increase
27 at lower concentrations. We demonstrate that positively biased NO_3^- and SO_4^{2-} measurements
28 result in overestimation of aerosol acidity and introduce non-trivial errors to ion balances of
29 inorganic aerosol. Though the source of the bias is uncertain, it is not corrected by the MARGA
30 online single-point internal LiBr standard. Our results show that calibration and verification of
31 instrument accuracy by multi-level external standards is required to adequately control analytical

32 accuracy. During the field intensive, the MARGA was able to capture rapid compositional

33 changes in $PM_{2.5}$ due to changes in meteorology and air mass history relative to known source

34 regions of PM precursors, including a fine NO_3^- aerosol event associated with intrusion of arctic

35 air into the southeast U.S.

36

37 1. Introduction

38

39   Secondary inorganic aerosols are formed from gaseous precursors including

40 ammonia (NH_3), nitric acid (HNO_3) and sulfur dioxide (SO_2), producing ammonium nitrate

41 (NH_4NO_3), ammonium bisulfate (NH_4HSO_4) and ammonium sulfate (($NH_4)_2SO_4$) particles.

42 These gaseous precursors and particulate matter, which partition between phases to establish a

43 thermodynamic equilibrium of ammonium-sulfate-nitrate (Finlayson-Pitts and Pitts, 2000;

44 Seinfeld and Pandis, 2006), represent a significant fraction of $PM_{2.5}$ (Seinfeld and Pandis, 2006;

45 Pinder et al., 2007) and contribute to atmospheric deposition of nutrients and acidity. The

46 implementation of National Ambient Air Quality Standards has reduced emissions of NO_x and

47 SO_2; however, NH_3 is not regulated and has not been routinely monitored until relatively

48 recently (Puchalski et al, 2015). Nevertheless, to further reduce fine particulate matter,

49 controlling NH_3 emissions has been suggested to be more cost-effective than further reductions

50 of NO_x and SO_2 in some cases, (Vayenas et al, 2005; Pinder et al., 2007). Reduction of NH_3

51 emissions may also represent the most effective strategy for reducing atmospheric nitrogen

52 deposition to acceptable levels (Li et al., 2016) in some ecosystems. High-frequency

53 simultaneous measurements of the gas and aerosol components of the ammonium-sulfate-nitrate

54 system are required to investigate inorganic aerosol characteristics (e.g., phase partitioning,

55 acidity) and formation processes and to quantify the dry component of nitrogen deposition.

56   Traditionally, integrated denuder and/or filter based techniques (i.e., 24 hours or longer)

57 have been used to monitor inorganic aerosols and their precursors (Trebs et al 2004 and

58 references therein; Benedict et al., 2013; Chen et al., 2014). The disadvantages of poor temporal

59 resolution and labor intensity as well as positive and negative sampling artifacts make these

60 methods difficult to deploy for extended periods of time and of limited use for characterization

61 of rapidly changing atmospheric conditions. Recent development of near real-time semi-

62 continuous analyzers, including the Particle-Into-Liquid sampler (PILS-IC, Metrohm AG,

63 Herisau, Switzerland), Particle-Collector-Ion Chromatograph (PC-IC), Aerosol Mass

64 Spectrometer (AMS, Aerodyne Research Inc., USA), Ambient Ion Monitor-Ion Chromatograph

65 (AIM-IC, URG Corp. And Dionex Inc., USA) and the Monitor for Aerosols and Gases in

66 Ambient Air (MARGA, Metrohm Applikon B.V., the Netherlands) facilitate monitoring

67 inorganic atmospheric constituents with much higher time resolution (Jayne et al., 2000; Weber

68 et al., 2001; Al-Horr et al., 2003; Trebs et al., 2004; Schaap et al., 2011; Markovic et al., 2012).

69 A version of the MARGA incorporating two sample boxes (MARGA 2S), similar to the system

70 described here, has recently been used to quantify dry deposition using a micrometeorological

71 gradient flux method (Rumsey and Walker, 2016).

72   MARGA's capability of near real-time (hourly) simultaneous measurement of water

73 soluble particulate species as well as their gaseous precursors makes it a state-of-art research

74 instrument. Such time-resolved measurements allow investigation of highly time sensitive,

75 rapidly changing pollution episodes as well as aerosol processes such as gas/particle partitioning

76 and neutralization state. The MARGA has been deployed in widely varying environments to

77 monitor ambient gaseous and particulate water soluble species including NH_3, SO_2, HNO_3,

78 NH_4^+, SO_4^{2-} and NO_3^- (Schaap et al., 2011; U.S. EPA, 2011; Makkonen et al., 2012; Mensah et

79 al., 2012; Khezri et al., 2013; Huang et al., 2013; Rumsey et al., 2014; Shi et al., 2014; Allen et

80 al., 2015; Twigg et al., 2015; Rumsey and Walker, 2016). Although the MARGA denuder and

81 steam jet aerosol collector (SJAC) have been evaluated for collection efficiency of gases and

82 particles (Wyers et al., 1993; Khlystov et al., 1995), there is relatively limited data on accuracy

83 and precision of concentration measurements (Weber et al., 2003; Trebs et al., 2004; Makkonen

84 et al., 2012; Lee et al., 2013; Rumsey et al., 2014; Allen et al., 2015). Phillips et al. (2013) found

85 that HNO_3 determined by the MARGA's wet rotating denuder displays a cross-sensitivity to

86 N_2O_5. The magnitude of the resulting positive bias in HNO_3 is highly dependent on the ambient

87 conditions (eg. NO_x, O_3, biogenic VOC concentrations and temperature) responsible for N_2O_5

88 production.   Lee et al. (2013) observed differences in SO_4^{2-}, NH_4^+ and NO_3^- at a suburban site in

89 Hong Kong where an AMS instrument measured only 33-60% of the PM mass measured by a

90 collocated MARGA. Part of the difference was attributed to different particle size cut of the

91 inlets used ($PM_{1.0}$ for AMS and $PM_{2.5}$ for MARGA).   Rumsey et al. (2014) compared the

92 MARGA to a reference time-integrated denuder/filter pack system. SO_2, SO_4^{2-} and NH_4^+ agreed

93 within 15% between the two systems; however, HNO_3 and NH_3 comparisons showed an

94 underestimation by MARGA of 30%, mostly likely due to loss to the surface of the long (≈ 4 m)

95   polyethylene sample tubing used. Though differences between the MARGA and other

96   measurement systems have been observed, the extent to which the differences may be

97   attributable solely to chromatorgraphy has not been evaluated.

98   The objective of this study is to evaluate MARGA performance with a focus on accuracy

99   and precision characteristics related to automated chromatography analysis. Specifically, we

100 investigate misidentification and misintegration by the MARGA software as well as errors and

101 uncertainties resulting from such issues. To aid efficiency and flexibility in the reprocessing of

102 MARGA chromatograms, an alternative chromatography procedure, based on offline analysis of

103 raw MARGA data, was employed. Using laboratory standards, analytical accuracy, precision,

104 and method detection limits derived from the two chromatograph processing methods were

105 compared. Field measurements were used to further evaluate instrument performance and to

106 demonstrate the ability of the MARGA instrument to resolve important atmospheric processes,

107 including diurnal patterns of observed gaseous (NH_3, SO_2, HNO_3) and particulate water soluble

108 species (NH_4^+, SO_4^{2-} and NO_3^-), fine particle neutralization state, and changes in atmospheric

109 composition related to synoptic meteorological patterns. Using aerosol neutralization state as a

110 case study, the impact of chromatography errors on measurement accuracy was assessed.

111

112 2. Methods and materials

113 2.1 MARGA system

114   Details and principles of the MARGA system have been previously described (Rumsey et

115 al., 2014; Rumsey and Walker, 2016). Briefly, the MARGA sampler box consists of a wet

116 rotating denuder (WRD) and a steam jet aerosol collector (SJAC), which enables semi-

117 continuous collection and measurement of gaseous and water soluble inorganic particulate

118 species in the ambient air. When drawn through the WRD, gaseous species are collected by

119 diffusion into a liquid film while particles pass through the WRD to the SJAC where super-

120 saturation grows the particles by condensation. Liquid samples from the WRD and SJAC are

121 continuously collected in individual syringes and analyzed by Ion Chromatography (IC) on an

122 hourly basis at the detector unit. Cation and anion sample loop volumes are 500 µl and 250 µl,

123 respectively. By employing two sets of liquid syringes, a set of samples is collected while

124 samples from the previous hour are analyzed. To monitor accuracy and automatically adjust

125 concentrations, liquid samples are mixed with an internal lithium bromide (LiBr) standard at a

126 fixed ratio before injection for IC analysis.

127

128   2.2 Chemical materials

129   DI water (18.2 MΩ·cm, Milli-Q Reference system, Millipore) with 10 ppm H_2O_2 (30%

130   certified ACS grade, Fisher Scientific) was used as absorbance solution for the MARGA WRD

131   and SJAC sample collection. H_2O_2 was added to prevent bacteria growth and subsequent loss of

132   NH_4^+. The MARGA internal standard LiBr (>99%, ACROS Organics) aqueous solution was

133   prepared at concentrations of 320µg/L Li^+ and 3680 µg/L Br^-. Solid chemical standards

134   NH_4NO_3, NH_4Cl, $(NH_4)_2SO_4$, $NaNO_3$, KCl, $CaCl_2 \cdot 2H_2O$ and $MgSO_4 \cdot 7H_2O$ (≥99% certified

135   ACS grade, Fisher Scientific) were used to prepare stocks and various levels of liquid external

136   standards. Certified aqueous analytical standard solutions purchased from Alltech Associates

137   (Anion Mix 1, Cation Mix B, Alltech Associates, Inc) served as accuracy check standards. We

138   note here that "internal" standard refers to the MARGA LiBr standard that is mixed with every

139   MARGA liquid sample immediately upstream of the IC injection loop. "External" standards

140   refer to liquid standards that are introduced at the WRD and SJAC, as described in more detail

141   below.

142

143   2.3 Chromatography

144   MARGA proprietary chromatography software consists of an online version used for

145   automated analysis when the instrument is in measurement mode and a "MARGA tool", so

146   named by the manufacturer, used for offline analysis of chromatograms, either individually or in

147   batches, but otherwise identical to the online version. In both cases, liquid analyte concentrations

148   are determined by calculating the total amount of injected sample directly from the conductivity

149   measurement following the method of van Os et al. (1984). As mentioned previously, accuracy

150   is controlled by adjusting the measured concentration based on a single point internal LiBr

151   standard, at a working concentration of 320 µg/L of Li^+ and 3680 µg/L of Br^-, which is injected

152   with each sample. The MARGA software does not employ a multipoint calibration curve.

153   During post processing of field data, it was discovered that peaks integrated by the

154   MARGA tool showed a certain degree of misidentification and inconsistent integration. Specific

155   integration issues include incorrectly defined baseline due to peak fronting and tailing and

156   shifting between "drop perpendicular" and "valley to valley" integration options among samples

157   (shown in Supplemental Information). As indicated by the examples shown in Supplemental

158 Information, baseline selection by the MARGA tool could vary from sample run to run, which

159 could introduce significant errors and uncertainties. Integration issues are particularly

160 problematic when the IC analytical columns deteriorate due to extended use. Under such

161 conditions, unresolved peaks occurred more frequently.

162 In addition to misidentification and misintegration issues with the MARGA software,

163 reintegration of individual peaks with the MARGA tool was found to be inefficient and

164 inflexible. Although the MARGA tool contains adjustable integration parameter settings such as

165 peak search sensitivity and peak search smoothing, the parameters are applied to all

166 chromatograms. For example, the adjusted parameter may achieve the desired integration for a

167 particular misintegrated peak, but other peaks which were deemed as integrated properly prior to

168 any adjustments may subsequently be improperly integrated. The inability to manually adjust

169 the integration for individual peaks makes post-processing of chromatograms time consuming.

170 Hence, an alternative chromatography software (Chromeleon V7.2, Thermo Scientific Dionex)

171 was tested for reprocessing of MARGA chromatograms.

172 In order to import MARGA generated chromatograms to the Chromeleon

173 chromatography data processing system, raw MARGA chromatography data (.dat format) were

174 converted to time series of conductivity (.txt format) using the MARGA tool. Using the

175 Chromeleon generated template (.cdf format) file, as well as a custom Java script, a batch of

176 MARGA conductivity time series (.txt format) files are converted to their corresponding .cdf

177 format. A folder of conductivity data files in cdf format is then imported to Chromeleon for

178 chromatogram reprocessing.

179 MARGA and Chromeleon approaches were compared in terms of peak areas and

180 calculated concentrations of internal and external liquid standards, as well as determinations of

181 laboratory blanks, method detection limits, and air concentrations during ambient sampling. To

182 compare integration characteristics between the MARGA tool and Chromeleon software, a series

183 of external liquid standards (Table S1), representing a range of concentrations equivalent to ≈

184 $0.05 - 10.5 \ \mu g/m^3 \ NH_4^+$, NO_3^- and SO_4^{2-} in air, were run through the MARGA instrument with

185 the air pumps and SJAC steam generator disconnected. This configuration allowed liquid

186 standards to pass through the entire sampling (i.e., WRD and SJAC and liquid sampling lines)

187 and analytical (i.e., syringes and ICs) components of the system. The resulting chromatograms

188 were used to generate a calibration curve using Chromeleon, in which peak areas were related to

189   liquid standard concentration (µg/L). These peak areas and concentrations were then compared

190   directly to peak areas and concentrations generated by the MARGA software (without any

191   further manual peak integration adjustment), the latter being adjusted only by the internal LiBr

192   standard. A certified accuracy check standard was used to evaluate the accuracy of the

193   calibration curves generated by Chromeleon and all of the analytes were found to be within the

194   10% accuracy check criteria. System blanks using absorbance solution were evaluated in the

195   same manner as the external liquid standards. Finally, both the MARGA internal standard (LiBr)

196   and a subset of the external standards were verified by independent analysis on a Dionex ICS-

197   2100 (Thermo Scientific, Waltham, MA) multi-point calibrated with additional certified

198   standards. Due to different loop size and corresponding detection limit of the Dionex system,

199   only a subset of the external standards was independently verified.

200

201   2.4. Field study

202   Field measurements were conducted in a grass field at the Blackwood Division of Duke

203   Forest (35.98ºN, 79.09ºW) near Chapel Hill, NC. Duplicate MARGA sample boxes (SB1 and

204   SB2) were positioned in parallel (i.e., collocated) with inlets ≈ 1.5 m above the ground. Both

205   MARGA sample boxes employed a Teflon coated cyclone-type inlet with an aerodynamic 2.5

206   µm cut size at a flow rate of 16.7 LPM (URG-2000-30EH, University Research Glassware

207   Corporation). A short (0.2 m) length of 25.4 mm O.D. Teflon tubing connected the atmospheric

208   inlet to the MARGA denuder. MARGA sampler and detector boxes were equipped with weather

209   protection enclosures which were temperature controlled at 25ºC.

210   Sampler air flow rates were measured and verified weekly by connecting a NIST

211   traceable primary standard flow meter (Bios DryCal DC-Lite flowmeter, Mesa Laboratories,

212   Inc., Lakewood, CO) to the sampler inlets. Based on the calibration by the flow meter, MARGA

213   reported flow rates were overestimated by 6% and 8% for sample box 1 (SB1) and 2 (SB2),

214   respectively, and air concentrations were adjusted accordingly. Initial data validation was

215   conducted by monitoring the MARGA automated status codes; data with internal standard LiBr

216   responses outside of ±10% nominal concentrations were invalidated and excluded from further

217   analysis.

218   To compare air concentrations derived from MARGA and Chromeleon software, the

219   liquid calibration curves (see above section 2.2) generated by Chromeleon were used to calculate

7

220 liquid concentrations, and by combining with air and liquid flow rates, corresponding air

221 concentrations were derived. The Chromeleon derived air concentrations were then compared to

222 air concentrations generated by the MARGA software, which used only the internal LiBr

223 standard as a calibration adjustment. For this comparison, the same air and liquid flow rates were

224 used. Both sets of air concentrations were corrected for system blanks and air flow rate

225 calibrations. The MARGA was operated continuously in the field from 15 October to 17

226 November 2014. However, due to a failure of the IC degasser unit, no valid data were generated

227 from 31 October to 2 November 2014.

228

229 2.5. Ancillary field data

230   A 10 m meteorological station is maintained and managed at Duke Forest by the North

231 Carolina Division of Forest Resources and Bureau of Land management. Verified hourly

232 metrological data were obtained online: (http://mesowest.utah.edu). Concentrations of $PM_{2.5}$

233 mass (TEOM model 1400ab, R&P Thermo Scientific, Franklin, MA) and organic/elemental

234 carbon (OC/EC, Model 4 Semi-continuous field analyzer, Sunset Laboratory, Inc., Hillsborough,

235 NC) were measured adjacent to the MARGA instrument. Backward air mass trajectories were

236 calculated for select periods using the Hybrid Single Particle Lagrangian Integrated Trajectory

237 (HYSPLIT) model (Draxler and Rolph, 2003) with NOAA ARL EDAS 40 km meteorological

238 data. Trajectories were run for 168 hour periods at an arriving height of 500 m above the ground

239 level. To aid interpretation of the back trajectories, facility emission inventory data for NO_x, SO_2,

240 and NH_3 were retrieved from the 2011 National Emission Inventory database

241 (http://www.epa.gov/ttn/chief/net/2011inventory.html).

242

243 3   Results and discussion

244 3.1. Laboratory study of chromatography characteristics

245   MARGA chromatograms were systematically examined by running a series of liquid

246 external standards over a range of concentrations listed in Table S1. Each standard level was

247 analyzed for approximately 20 hours, producing $N = 80$ observations for 4 analytical channels

248 combined (two sample boxes for gas and aerosol channels). The same sets of chromatograms

249 were re-processed by Chromeleon to generate multi-point calibration curves for each analyte.

250 Peaks that were obviously misintegrated by the MARGA tool were not included in this analysis.

251   Relationships between peak area and standard concentration were linear except for SO_4^{2-}, for

252   which a polynomial fit was adopted to better represent the entire concentration range. All

253   calibration curves had r^2 values > 0.999. A certified check standard was used to evaluate the

254   accuracy of the calibration curves generated by Chromeleon and all analytes were found to be

255   within the 10% accuracy check criteria. Using absorbance solution to assess contamination,

256   blank concentrations of NO_3^- and SO_4^{2-} reported by Chromeleon were 0.002 and 0.080µg/m^3,

257   respectively, while the corresponding system blanks determined by the MARGA tool were 0.018

258   and 0.109 µg/m^3. NH_4^+ was not detectable in the blank solution.

259   Table 1 lists estimated method detection limits for the species of interest calculated using

260   both the MARGA tool and Chromeleon. Method detection limits were calculated as

261   2.58×standard deviation of the lowest detectable external standards, a statistical method

262   described in detail by Currie (1999). Method detection limits calculated using the MARGA

263   software are substantially larger than corresponding detection limits calculated with Chromeleon,

264   indicating more variability in the MARGA integrations from sample to sample. Such

265   inconsistency will translate to larger uncertainties for low concentration samples. This is

266   particularly important when attempting to resolve very small differences between two MARGA

267   sample boxes, a requirement for flux gradient applications (Rumsey and Walker, 2016). Error

268   propagations inherited from misintegration could be minimized by reexamining the

269   chromatograms. We note that the detection limits of the instrument evaluated here are larger,

270   particularly for anions, than those reported by Rumsey and Walker (2016), which used the same

271   MARGA software but a different instrument. This indication of variability demonstrates the

272   need to characterize individual measurement systems. The detection limits calculated with

273   Chromeleon are more similar to those reported by Rumsey and Walker (2016).

274   Table S2 lists the internal standard peak areas as integrated by the MARGA tool and

275   Chromeleon for each of the corresponding external standard levels. Note that while the

276   concentrations of anions and cations in the external standards vary by level, the actual

277   concentration of the internal standard does not. For both Li^+ and Br^-, systematically larger peak

278   areas are calculated by the MARGA software. While the systematic difference for Br^- is rather

279   consistent (17%), differences in Li^+ between the two software techniques decrease with

280   increasing external standard concentration. As the peak areas of Na^+ and NH_4^+ increase, the close

281   retention times of Na^+, NH_4^+, and Li^+ cause the peaks to appear more like unresolved lumps (i.e.,

282   peak merging effect). At these higher standard concentrations, the MARGA software

283   underestimates the Li^+ peak area relative to Chromeleon integration from sample to sample

284   becomes less consistent. This is likely due to the MARGA software frequently shifting between

285   "drop perpendicular" and "valley to valley" integration options between samples, introducing

286   more variability to the calculated areas (see Supplemental Information Figure S1). For

287   consistency, the "drop perpendicular" integration option was adopted for all Chromeleon

288   reprocessing. We observed that as the concentration levels increase, the errors due to adopting

289   different integration options could be as much as 6% at the highest external standard

290   concentration equivalent to ≈ 10.5 µg/m^3. In summary, the consistent 17% difference in Br^- peak

291   areas between software packages is not necessarily a source of error in the final calculation of

292   MARGA liquid concentrations. For Li^+, the variability in integration and decrease in the

293   difference in peak area between the two software packages at higher standard levels would

294   translate to systematic differences in corresponding NH_4^+ liquid concentrations above ≈ 100

295   µg/L (≈ 2.5 µg/m^3 in air).

296   In addition to underestimation of Li^+, other issues associated with MARGA processing of

297   cation chromatograms include misidentification of NH_4^+ as Na^+ when a negligible Na^+ peak

298   existed and misidentification of NH_4^+ and Na^+ peaks together as a single NH_4^+ peak. For anion

299   chromatograms, NO_3^- peaks were rather frequently discovered as not identified at all; SO_4^{2-}

300   peaks were found to have an incorrectly defined baseline due to peak fronting and tailing (see

301   Supplemental Information Figures S2 - S5). These issues become more prevalent with column

302   age.

303

304   3.2 Field study

305   In order to assess the potential impact of chromatography related analytical errors

306   observed during the laboratory evaluation, MARGA performance was further investigated during

307   a one-month field campaign. Air concentrations generated by the MARGA tool and Chromeleon

308   are compared over a range of chemical and meteorological conditions, using particle

309   neutralization state as a case study. Intrusion of artic air into the southeast U.S. provided an

310   opportunity to observe rapidly changing and distinct patterns of gas-to-particle partitioning

311   within the ammonium-nitrate-sulfate system. In the following sections, air concentrations

312   presented in time series and summary statistics describing ambient measurements were generated

313   by Chromeleon unless otherwise indicated.

314   3.2.1 MARGA accuracy

315   Chromatograms reprocessed by the MARGA tool were individually examined and

316   concentrations were filtered for periods of instrument malfunction, peak misintegration, and LiBr

317   internal standard outside ±10% of the nominal target concentration. This filtering procedure

318   would include low concentrations in which there was an obvious problem with the original peak

319   integration. Filtered data were not included in the comparison between the MARGA tool and

320   Chromeleon. Table S3 presents the percentage of data excluded from the comparison. NO_3^-

321   peaks appeared to be the analyte most affected, especially in the case of HNO_3 (up to 6.2% of the

322   data). At sampling sites where HNO_3 concentrations are typically below $1\mu g/m^3$, data rejection

323   may be more extensive.

324   Air concentrations derived from the MARGA and Chromeleon software approaches were

325   compared by ordinary least squares regression using Chromeleon as the reference (Figure 1).

326   Over the entire range of conditions, concentrations calculated using the MARGA tool were

327   within 5% (slopes, Figure 1), on average, of those reported by Chromeleon for SO_4^{2-}, SO_2, NH_4^+

328   and NH_3.   Very good agreement is observed for NH_4^+ and NH_3, with slopes close to unity and

329   intercepts near zero. As concentrations were below 2.5 $\mu g/m^3$, potential disagreement resulting

330   from differences in cation integration at higher concentrations (section 3.1) was not observed.

331   Although the accuracy of NO_3^- was poorer, it was within 10%, overall. By contrast, HNO_3

332   concentrations, which were mostly below 1.0 $\mu g/m^3$, showed a positive bias of approximately

333   30%. Correlation of HNO_3 between the MARGA tool and Chromeleon also revealed a more

334   scattered pattern compared to other analytes. The 30% positive bias in MARGA HNO_3 results is

335   also observed for NO_3^- concentrations below $\approx 1.0 \mu g/m^3$ (Supplemental Information Figure S6).

336   Restricting the NO_3^- regression comparison to lower concentrations results in slopes of ≈ 1.4 and

337   1.5 over concentration ranges of $0 – 0.5 \mu g/m^3$ and $0 – 0.25 \mu g/m^3$, respectively, with intercepts

338   near zero; the disagreement increases at concentrations below $0.25 \mu g/m^3$. SO_2 and SO_4^{2-} results

339   also show positive bias in the MARGA results at lower concentrations, though not as large as

340   observed for HNO_3 and NO_3^-. For SO_2, slopes of ≈ 1.1, 1.15, and 1.2 are observed over

341   concentration ranges of $0 – 1.0 \mu g/m^3$, $0 – 0.5 \mu g/m^3$, and $0 – 0.25 \mu g/m^3$, respectively, with

342   intercepts near zero. Agreement improves at concentrations above 1.0 $\mu g/m^3$ as the slope

343 approaches unity. Over the entire range of conditions, SO_4^{2-} also shows good agreement, on

344 average, though with a significant offset (0.14 µg/m^3, Figure 1). At lower concentrations

345 (Supplemental Information Figure S6), a pattern of disagreement similar to SO_2 emerges; over

346 the range 0 – 1.0 µg/m^3, a slope and intercept of 1.09 and 0.09 are observed, respectively.

347 Similar discrepancy patterns were observed for SO_4^{2-} and NO_3^- when lower level external

348 standards were tested. In contrast to anions, cation results showed consistently good agreement

349 even at low concentrations.

350   The source of bias between the MARGA and Chromeleon results may result from several

351 factors: 1) MARGA overestimation from incorrectly defined peak start and end points due to

352 peak fronting and tailing; 2) incorrect baseline definition for smaller peaks (i.e., low observed

353 HNO_3 and NO_3^- concentrations) as compared to larger peaks; or perhaps the most likely

354 explanation, 3) inability of the van Os method used by the MARGA software to fully linearize

355 the relationship between peak area and liquid concentration at low concentrations. As noted

356 above, the method of van Os et al. (1984) for anion analysis with chemical suppression allows

357 calculation of the sample concentration directly from the conductivity measurement. van Os et

358 al. concluded that relationships between the amount of sample injected and total peak area were

359 linear over the range 2.0 – 40.0 mg/L. It was noted, however, that calculated concentrations at

360 the 1.0 mg/L standard level, the lowest concentration tested, were slightly low for NO_3^- and Cl^-

361 and slightly high for SO_4^{2-}. Subsequently, the 1.0 mg/L standard level was not used in the final

362 regression analysis used to test the linearity of the method. Accounting for differences in

363 injection loop size between studies, the 1.0 mg/L level used by van Os et al. (1984) is a factor of

364 2 to 2.5 larger than the highest standard concentration tested in our study (Table S1) and a factor

365 of 25 (SO_2) to 125 (HNO_3) larger than the corresponding average observed air concentrations

366 (Table 2). It is possible that the method of van Os et al. (1984) systematically over-predicts

367 anion concentrations at the lower concentrations observed in our study. This accuracy issue

368 would not be controlled by the single point Br^- internal standard (3680 µg/L), which is within the

369 linear response range of anion concentrations tested by van Os et al. (1984).

370   The NO_3^- bias observed here may help to explain the results of previous studies. Five

371 semi-continuous analyzers, which included an earlier version of a Wet-Annular Denuder/Steam-

372 Jet Aerosol Collector (Trebs et al., 2004, 2008) that predates the commercialized MARGA, were

373 evaluated and inter-compared by Weber et al. (2003) for measurements of NO_3^- and SO_4^{2-} in

374     $PM_{2.5}$ at the Atlanta EPA supersite. The earlier version MARGA analyzer showed a range of

375   25% to 34% significantly higher NO_3^- concentration as compared to a group mean of the five

376   semi-continuous monitors evaluated while measured SO_4^{2-} agreed well (within 10%). This

377   discrepancy was suspected to be a sampling artifact of NO_3^- formed from NO_x in the MARGA

378   particle steam collector, though there was a lack of correlation with measured NO_x. Four

379   instruments including a MARGA, an AMS, a denuder difference analyzer as well as an

380   integrated nylon filter based IMPROVE sampler were evaluated by Allen et al. (2015) during the

381   2013 Southern Oxidant and Aerosol Study (SOAS) campaign for particulate NO_3^-. The

382   MARGA measured much higher NO_3^- concentrations than the other three analyzers at this

383   southeastern US site where NO_3^- was mostly below 1.0 µg/m^3 during the sampling period.

384   Differences in inlet cyclone size cuts and cyclone efficiencies for supermicron particles may be

385   partly responsible. However, these examples of significantly higher MARGA NO_3^- relative to

386   other methods, as well as the results of this study, warrant further investigation of potential

387   chromatography related biases.

388

389   3.2.2 MARGA precision

390   Precision statistics (Table 2) were derived from orthogonal least squares regression (Wolff

391   et al., 2010) of concentrations from the two MARGA sample boxes operated in parallel (i.e.,

392   collocated). Orthogonal least squares acknowledges uncertainty in both the X and Y variables

393   (i.e. measurements from both sample boxes) and the standard deviation of the residuals of the

394   regression is therefore a measure of the overall precision of the MARGA system. Concentrations

395   of particulate NO_3^-, SO_4^{2-} , NH_4^+, gaseous SO_2 and NH_3 agree well between the sample boxes,

396   with slopes within 5% of unity and negligible intercepts (Table 2), indicating no significant

397   systematic differences between the two sample boxes. The standard deviations (precision) and

398   relative standard deviations (RSD, expressed as a percentage of the average air concentrations)

399   of the regression residuals reported here (µg/m^3) for NO_3^-, SO_4^{2-} , NH_4^+, and NH_3 are similar (<

400   10% RSD) to those reported by Rumsey and Walker (2016). The lower precision for SO_2

401   reported here is most likely related to larger differences in concentration between sample boxes

402   during periods of rapid concentration changes associated with the arctic air episode (Figures 2

403   and 3).

404   Relative to the other analytes, HNO_3 showed a much more significant difference between

405   the two sampler boxes (regression slope of 0.83). Additionally, HNO_3 precision (15.8% RSD)

406   was much lower than observed for NO_3^- aerosol (4.8% RSD) at nearly identical average

407   concentrations. These findings, in combination with the excellent agreement between sample

408   boxes for NO_3^-, suggest that the HNO_3 measurements were influenced by inlet, rather than

409   analytical, issues. As indicated by the much higher Henry's law coefficient of HNO_3 relative to

410   NH_3 and SO_2, HNO_3 is "sticky" and therefore more prone to inlet losses as well as re-evaporation

411   from inlet/tubing surfaces. Although the inlet cyclones used were Teflon coated, and the Teflon

412   tubing connecting the cyclone to the WRD was very short (0.2 m), our results suggest

413   differences in transmission efficiencies of the two inlets. Similar difficulties in sampling HNO_3

414   have been reported previously for studies in which size selective inlets and/or significant lengths

415   of sample tubing were used for MARGA sampling (Trebs et al., 2004; Rumsey et al., 2014;

416   Allen et al., 2015). In our study, the length of inlet tubing between the cyclone and WRD was

417   similar to the length of tubing (0.3 m) used by Rumsey and Walker (2016), the difference being

418   that no size selective inlet was used by Rumsey and Walker. In their study, multiple collocation

419   experiments showed much better agreement, on average, between the two sample boxes and

420   better precision (5.8% RSD), suggesting that the cyclone may be the primary source of

421   disagreement between sample boxes in the current study. It is important to note, however, that

422   concentrations of HNO_3 observed in the current study were generally very low, averaging 0.19

423    $\mu g/m^3$ over the study period. Such low concentrations contribute to greater relative variability

424   between sample boxes. Our results re-emphasize the requirement of low affinity tubing and inlets

425   with respect to both materials and surfaces/lengths for HNO_3 sampling.

426

427   3.2.3 Temporal patterns of gas and particle concentrations

428   Figure 2 shows time series of hourly gas phase concentrations of HNO_3, SO_2 and NH_3,

429   and particle phase NO_3^-, SO_4^{2-} and NH_4^+ (as local time (EDT)). From mid-October to mid-

430   November, meteorological conditions were mild and humid (Figure 3), which is typical of fall in

431   the southeast U.S. However, an arctic outbreak of cold air impacted the site from 13 to 17

432   November, accompanied by much lower temperature and relative humidity. Wind speed was

433   typical of the site, averaging 2 m/s. The prevailing wind directions were northwest and southwest

434   before the cold air period and northerly during the dry and cold period.

14

435   Figure 4 shows the diurnal pattern of gas and particle concentrations. Only days with

436   hourly data coverage greater than 65% were used for calculating diurnal profiles ($N = 26$). NH_4^+

437   and SO_4^{2-} exhibited a single mode pattern with a peak around 9-11 am local time. NO_3^- showed a

438   similar peak in the morning and a smaller peak at 9-11 pm. Morning peaks most likely represent

439   the downward mixing of aerosols from aloft when the nocturnal boundary layer breaks down.

440   The second peak of NO_3^- at night may be related to night time NO_3^- radical chemistry

441   (Finlayson-Pitts and Pitts, 2000; Seinfeld and Pandis, 2006) leading to formation of particulate

442   NO_3^-. The mid-afternoon (2-3pm) peak in gas phase HNO_3 results from photochemical

443   processing of NO_x. NH_3 showed a much broader afternoon peak, which may reflect local

444   emissions from natural sources during warmer afternoon periods. The diurnal pattern of SO_2

445   showed a pronounced peak around 10-11 am, and two less pronounced peaks at 8 pm and 1 am,

446   respectively. This pattern may reflect the competition between emission and dry deposition, as

447   well as boundary layer dynamics: higher emissions during the day versus slower dry deposition

448   rates and shallower boundary layer at night. The diurnal pattern is also affected by the large SO_2

449   spikes observed during the arctic air mass period, presumably associated with increased

450   emissions resulting from greater energy demand.

451   Gas/particle partitioning presented as fraction in the particle phase is shown in Figure 5.

452   In order to examine the aerosol neutralization state, chemical composition ratios were calculated

453   as:

454     $$R1 = \frac{NH_4^+}{SO_4^{2-}} \qquad\qquad (1)$$

455

456     $$R2 = \frac{NH_4^+}{NO_3^- + 2 \times SO_4^{2-}} \qquad\qquad (2)$$

457

458   where ratios R1 and R2 are molar concentration based. $R1 = 2$ reflects an aerosol entirely

459   composed of $(NH_4)_2SO_4$, which is the fully neutralized state of SO_4^{2-}. $R1 > 2$ indicates the

460   presence of NH_4NO_3 in addition to $(NH_4)_2SO_4$, while $R1 < 2$ signifies a state of NH_4^+ deficit

461   indicative of an acidic aerosol. Moreover, a ratio of $R2 = 1$ indicates a fully neutralized aerosol

462   containing NH_4NO_3 and $(NH_4)_2SO_4$, while $R2 > 1$ represents as condition of excess NH_4^+. A

463   value of $R2 < 1$ suggests acidic aerosol comprising NH_4NO_3 and a combination of NH_4HSO_4 and

464    $(NH_4)_2SO_4$ or, alternatively, NO_3^- associated with supermicron particles from aged sea salt or

465   crustal materials (Allen et al., 2015).

466   Two distinct periods of contrasting aerosol composition were observed (Figure 5d). With

467   R1 mostly less than 2 and R2 less than or close to 1, aerosol measured during October primarily

468   comprised NH_4HSO_4 and $(NH_4)_2SO_4$. When R1 approached 1 for three short episodes in October,

469   particles most likely existed solely as NH_4HSO_4. The observed acidity most likely suppressed

470   NO_3^- partitioning and formation, which is reflected by a significant decrease in the molar ratio of

471   NO_3^- in aerosol phase to as low as 0.1-0.2 (Figure 5a). Limited aerosol NO_3^- formation was also

472   reported by Allen et al. (2015) at a southeastern US (SOAS) site where aerosol was acidic. By

473   contrast, R1 was mostly above 2 in November, indicating the presence of NO_3^-. From 13 to 17

474   November, R1 reached as high as 4. Nevertheless, R2 was generally close to 1 during November,

475   indicating an aerosol comprised of NH_4NO_3 and $(NH_4)_2SO_4$. In contrast to the SO_4^{2-} dominated

476   October period, NO_3^- was a much greater contributor to inorganic aerosol in November; molar

477   concentrations of NH_4NO_3 even surpassed $(NH_4)_2SO_4$ when R1 reached 4 during the cold air

478   event. It should be noted that only acidity from inorganic species was examined in this study and

479   the ion balance could be further affected if organic acids were present and taken into account.

480   As noted above and illustrated in Figure S6, a positive bias in NO_3^- and SO_4^{2-} resulting

481   from peak integration and processing with the MARGA tool is observed for air concentrations

482   below ~ 1.0 $\mu g/m^3$. Our field study provides an opportunity to quantify the impact of these errors

483   over a range of chemical and meteorological conditions. For this analysis, the difference

484   between hourly concentrations determined by the MARGA versus Chromeleon software was

485   calculated as a percent relative to the Chromeleon result (i.e., 100%·(MARGA-

486   Chromeleon)/Chromeleon). Overall statistics of the hourly relative differences are summarized

487   in Figure 5e, including differences in phase partitioning (i.e., molar ratios calculated as

488   particle/(particle+gas)) and neutralization state (R1 and R2). As expected, differences in the

489   NH_4^+/NH_3 partitioning ratio are near zero because no bias was observed between Chromeleon

490   and MARGA derived concentrations of NH_3 and NH_4^+. Average and median differences in the

491   SO_4^{2-}/SO_2 partitioning ratio were similarly small, which is expected given that average SO_4^{2-}

492   and SO_2 concentrations were 1.41 and 0.98 $\mu g/m^3$, respectively (Table 2). These concentrations

493   are above the level at which biases between MARGA and Chromeleon become significant. Mean

494   and median differences in the NO_3^-/HNO_3 partitioning ratio were ≈ -10% and -1.5%,

495 respectively, indicating a smaller ratio calculated with the MARGA software. As shown in

496 Figure 5e, the NO_3^- /HNO_3 partitioning ratio exhibits much larger hourly variability relative to

497 the other analytes, reflecting a combination of larger concentration bias and random error

498 associated with integration of very small peaks. The average relative difference in R1 was ≈ -

499 13%, resulting from the combination of a constant offset and concentration dependent difference

500 between MARGA versus Chromeleon SO_4^{2-} results (section 3.2.1). Differences in R1 increase

501 non-linearly with decreasing SO_4^{2-} concentration, reaching ≈ -25% at 0.5 µg SO_4^{2-} /m^3. The

502 average relative difference in R2 was ≈ -14%, also exhibiting larger differences at lower

503 concentrations. Following the propagation of error in R2, differences are primarily driven by

504 much higher absolute concentrations of SO_4^{2-} relative to NO_3^-. Though absolute differences are

505 larger for NO_3^- concentrations, low concentrations result in a lesser contribution to the overall

506 difference in R2 between the MARGA and Chromeleon methods.

507

508 3.2.4 Arctic event

509   As noted above, an arctic outbreak of cold air impacted the site from 13 to 17 November.

510 The average temperature dropped from 12.9°C to 4.5 °C during this period, with a minimum of -

511 3.9°C, which is well below normal for this site. RH ranged from 21 to 77% during the cold air

512 event. Total concentrations of gases plus particles were ≈ 2X higher during the cold arctic event

513 for NH_3 and NH_4^+, SO_4^{2-} and SO_2; while for NO_3^- and HNO_3, a factor of 5 difference was

514 observed (summary shown in Table 3). Though air was drier during the arctic event,

515 temperatures were cold enough to drive partitioning of gas phase inorganic compounds towards

516 the particle phase. In addition to elevated NO_3^- concentrations, three distinct episodes of SO_2

517 occurred, with a maximum concentration of 32.56 µg/m^3 (Figure 2). Back trajectory analysis

518 (see Supplemental Information Figure S7) suggests that these SO_2 events reflect transport of

519 emissions from power plants and other point sources in the mid-west (see facility SO_2 emission

520 inventories Figure S8 in Supplemental Information). SO_2 from more local sources during the

521 extremely dry and cold arctic air conditions might also have contributed to the observed SO_2

522 spikes.

523   Gas and particle chemistry during the 13 to17 November period, including TEOM $PM_{2.5}$

524 mass and elemental/organic (EC/OC) carbon concentrations, are examined in more detail in

525 Figure 6. This four-day period represents the highest concentrations of SO_4^{2-}, NH_4^+, NO_3^- and OC

526 concentrations, as well as lowest temperature, observed during the study. However, total $PM_{2.5}$

527 mass showed less variability than the other species. Summaries of concentrations of gaseous and

528 particulate species are presented in Table 3 during and outside of the cold air event. In order to

529 better examine the arctic air mass intrusion, three sub-periods were selected, featuring a high

530 SO_4^{2-} episode; high NH_4^+ and NO_3^- episode; and a high OC episode (individual periods are

531 marked and color coded in Figure 6). Inorganic components in particles demonstrated a pattern

532 of high concentrations for periods1 and 2, while less so during period 3. Particulate organic

533 composition as represented by OC showed an opposite pattern, peaking in period 3. Differences

534 in time resolved concentrations of inorganic and organic species illustrate different emission

535 sources for inorganic and organic particulate pollutants. Back trajectories associated with the

536 three episodes are presented in Figure 6. For inorganic episodes 1 and 2, air masses originated

537 from the arctic and passed through the U.S. mid-west and Ohio River valley where emissions of

538 inorganic aerosol precursors, SO_2 and NO_x, from power plants and heavy industries were

539 encountered. Gas phase NH_3 concentrations are very low during these episodes, with the

540 majority of NHx in the particle phase. By contrast, trajectories associated with the high OC

541 episode (period 3) suggest more of a northeastern origin and perhaps a greater influence of

542 residential wood burning associated with cold temperatures. During periods 1 and 2, inorganic

543 compounds contributed the majority of $PM_{2.5}$ mass. The estimated sum of inorganics including

544 SO_4^{2-}, NO_3^- and NH_4^+ accounted for 61±31% and 83±24%, respectively of the $PM_{2.5}$ mass for

545 period 1 and 2. In contrast, inorganic compounds only accounted for 22±11% of $PM_{2.5}$ mass

546 during period 3.

547

548 4   Summary and conclusions

549   The MARGA is a state-of-art instrument that measures near real-time water soluble

550 particulate species as well as their gaseous precursors. The current commercial version of the

551 MARGA incorporates a continuous internal standard (LiBr) to verify and calibrate instrument

552 response for automated data generation and reporting. Close examination of MARGA

553 chromatograms revealed a number of issues, including misidentification and misintegration of

554 analyte peaks. Peak integration across similar chromatograms was found to be inconsistent with

555 the MARGA software shifting between integration options "drop perpendicular" and "valley to

556 valley" among samples. In addition, NO_3^- peaks were rather frequently discovered as not

557 integrated or identified; SO_4^{2-} peaks were found to have an incorrectly defined baseline due to

558 peak fronting and tailing. Adjustment of individual peak integrations was found to be difficult

559 and inefficient with features provided by MARGA tool software. Hence, an alternative

560 integration software, Chromeleon by Thermo Scientific Dionex, was used to reprocess the raw

561 chromatograms. A custom Java script was developed to incorporate MARGA raw conductivity

562 data into Chromeleon for reprocessing.

563 Though a number of chromatography issues with the MARGA commercial software were

564 identified, a relatively small percentage (6.2%) of data, overall, were invalidated due to peak

565 misintegration issues during the one-month field study described here. NO_3^- peaks appeared to be

566 the analyte most affected and higher rates of data invalidation may be expected where NO_3^-

567 concentrations are typically low. The additional flexibility and consistency of Chromeleon in

568 integrating small peaks results in lower method detection limits relative to the MARGA

569 chromatography software. Very good agreement between the two chromatography methods was

570 observed for cations across the range of observed ambient concentrations and for anions at

571 concentrations above $\sim 1\mu g/m^3$. At ambient concentrations below ~ 1 $\mu g/m^3$, however,

572 concentrations determined using the MARGA software are biased +30% and +10% for NO_3^- and

573 SO_4^{2-}, respectively, compared to concentrations determined using the alternative chromatography

574 procedure. Differences between the two methods increase at lower concentrations. Over the

575 range of conditions observed in our field study, the bias in NO_3^- produces non-trivial errors in

576 average NO_3^- concentrations and metrics of particle acidity. While the cause of this bias is

577 unclear, we make the following recommendations for controlling accuracy:

578 - Do not rely solely on the LiBr internal standard to ensure accuracy of the
579   chromatographic analysis

580 - Calibrate with multi-point curves using external liquid standards
581 - Use a range of external standards appropriate for expected ambient concentration levels
582   and for resolving potential non-linearity in detector response at low concentrations

583

584 During the field campaign, the MARGA captured rapid compositional changes in

585 $PM_{2.5,}$ including changes in neutralization state. A particularly high NO_3^- episode associated with

586 arctic air mass intrusion and transport of pollutants from sources in the mid-west U.S. was

587 observed. Our field study further demonstrates the usefulness of the MARGA system for

588 characterizing the temporal characteristics of the sulfate-nitrate-ammonium system associated

589 with changes in local (i.e., diurnal) and synoptic scale interactions between meteorology,

590 emissions, and aerosol processing.

591

592 **Acknowledgements**

593

600

601 **Description of Supplemental Information**

602 Table of multi-level external standards and certified standard; table of peak areas of internal LiBr

603 standard as integrated by MARGA tool and Chromeleon for different external standard levels;

604 table of fraction of data points invalidated due to misidentification and misintegration by

605 MARGA tool; figures showing examples of misidentification and misintegration by MARGA

606 tool; figure showing comparison of Chromeleon and MARGA tool in field samples at low

607 concentrations of SO_4^{2-} and NO_3^-; figure of corresponding back trajectories of three SO_2

608 episodes; figure of SO_2 point source emission inventory map (2011) covering middle and eastern

609 US.

610 **References**

611 Al-Horr, R., Samanta, G., and Dasgupta, P.K., 2003. A continuous analyzer for soluble anionic

612 constituents and ammonium in atmospheric particulate matter. Environ. Sci. Tech., 37, 5711-

613 5720.

614

615 Allen, H.M., Draper, D.C., Ayres, B.R., Ault, A., Bondy, A., Takahama, S., Modini, R.L.,

616 Baumann, K., Edgerton, E., Knote, C., Laskin, A., Wang, B., and Fry, J.L., 2015. Influence of

617 crustal dust and sea spray supermicron particle concentrations and acidity on inorganic NO3-

618 aerosol during the 2013 Southern Oxidant and Aerosol Study. Atmos. Chem. Phys., 15, 10669-

619 10685.

620

621 Benedict, K.B., Chen. X., Sullivan, A.P., Li, Y., Day, D., Prenni, A.J., Levin, E.J.T.,

622 Kreidenweis, S.M., Malm, W., Schichtel, B.A., Collett, J.L., 2013. Atmospheric concentrations

623 and deposition of reactive nitrogen in Grand Teton National Park. J. Geophy. Res., 118, 11875-

624 11887.

625

626 Chen, X., Day, D., Schichtel, B., Malm, W., Matzoll, A.K., Mojica, J., McDade, C.E., Hardison,
627 E.D., Hardison, D.L., Walters, S., Van De Water, M., Collett, J.L., 2014. Seasonal ambient
628 ammonia and ammonium concentrations in a pilot IMPROVE NHx monitoring network in the
629 western United States. Atmos. Environ., 91, 118-126.
630

631 Currie, L. 1999. Nomenclature in evaluation of analytical methods including detection and
632 quantification capabilities (IUPAC Recommendations 1995). Analytica Chimica Acta., 391,105-
633 126.
634

635 Draxler, R.R., Rolph, G.D., 2003. HYSPLIT (hybrid single particle Lagrangian integrated
636 trajectory) model access via website (http://www.arl.noaa.gov/ready/hysplit4.html). NOAA Air
637 Resources Laboratory, Silver Spring, MD.
638

639 Finlayson-Pitts,B.J., and Pitts, J.N., 2000. Chemistry of the upper and lower atmosphere.
640 Academic Press, New York, 2nd edition.
641

642 Huang, Y., Li, L., Li, J., Wang, X., Chen, H., Chen, J., Yang, X., Gross, D.S., Wang, H., Qiao,
643 L., and Chen, C., 2013. A case study of the highly time-resolved evolution of aerosol chemical
644 and optical properties in urban Shanghai, China.   Atmos. Chem. Phys., 13, 3931-3944.
645

646 Jayne, J.T., Leard, D.C., Zhang, X., Davidovits, P., Smith, K.A., Kolb, C.E., Worsnop, D.R.,
647 2000. Development of an Aerosol Mass Spectrometer for size and composition analysis of
648 submicron particles. Aerosol Sci. Tech., 33, 49-70.
649

650 Khezri, B., Mo, H., Yan, Z., Chong, S-L., Heng, A.K., and Webster, R.D., 2013. Simultaneous
651 online monitoring of inorganic compounds in aerosols and gases in an industrialized area.
652 Atmos. Environ., 80, 352-360.
653

654 Khlystov, A., Wyers, G.P., and Slanina, J., 1995. The steam-jet aerosol collector.
655 Atmos. Environ., 29, 2229-2234.
656

657 Lee, B.P., Li, Y.J., Yu, J.Z., Louie, P.K.K., and Chan, C.K., 2013. Physical and chemical
658 characterization of ambient aerosol by HR-ToF-AMS at a suburban site in Hong Kong during
659 springtime 2011. J. Geophys. Res., 118, 8625-8639.
660

661 Li, Y., Schichtel, B.A., Walker, J.T., Schwede, D.B., Chen, X., Lehmann, C.M.B.,
662 Puchalski, M.A., Gay, D.A., Collett, J.L., 2016. Increasing importance of deposition of reduced
663 nitrogen in the United States. Proceedings of the National Academy of Sciences, 113, 5874-
664 5879.
665

666 Markovic, M.Z., VandenBoer, T.C., and Murphy J.G., 2012. Characterization and optimization
667 of an online system for the simultaneous measurement of atmospheric water-soluble constituents
668 in the gas and particle phases. J. Environ.Monit., 14, 1872-1884.
669

670   Makkonen, U., Virkkula, A., Mäntykenttä, J., Hakola, H., Keronen, P., Vakkari, V., and
671   Aalto, P. P., 2012. Semi-continuous gas and inorganic aerosol measurements at a Finnish urban
672   site: comparisons with filters, nitrogen in aerosol and gas phases, and aerosol acidity. Atmos.
673   Chem. Phys., 12, 5617-5631.
674

675   Mensah, A.A., Holzinger R., Otjes, R., Trimborn, A., Mentel, T.F., ten Brink, H., Henzing, B.,
676   and Kiendler-Scharr, A., 2012. Aerosol chemical composition at Cabauw, The Netherlands as
677   observed in two intensive periods in May 2008 and March 2009. Atmos. Chem. Phys., 12, 4723-
678   4742.
679

680   Phillips, G.J., Makkonen, U., Schuster G., Sobanski, N., Hakola, H., Crowley, J.N., 2013. The
681   detection of nocturnal N_2O_5 as HNO_3 by alkali and aqueous-denuder techniques. Atmospheric
682   Measurement techniques 6, 231-237.
683

684   Pinder,R.W., Adams P.J., and Pandis S.N., 2007. Ammonia emission controls as a cost-effective
685   strategy for reducing atmospheric particulate matter in the Eastern United States. Environ. Sci.
686   Technol., 41, 380-386.
687

688   Puchalski, M.A., Rogers, C.M., Baumgardner, R., Mishoe, K.P., Price, G., Smith, M.J., Watkins,
689   N., and Lehmann, C.M., 2015. A statistical comparison of active and passive ammonia
690   measurements collected at Clean Air Status and Trends Network (CASNET) sites. Environ Sci
691   Processes & Impacts, 17, 358-369.
692

693   Rumsey, I., Cowen, K., Walker, J.T., Kelley, T.J., Hanft, E.A., Mishoe, K., Rogers, C., Proost,
694   R., Beachley, G.M., Lear, G., Frelink, T., and Otjes, R.P., 2014. An assessment of the
695   performance of the Monitor for AeRosols and GAses in ambient air (MARGA): a semi-
696   continuous method for soluble compounds. Atmos. Chem. Phys., 14, 5639–5658.
697

698   Rumsey, I., and Walker, J.T., 2016. Application of an online ion-chromatography-based
699   instrument for gradient flux measurements of speciated nitrogen and sulfur. Atmos. Meas. Tech.,
700   9, 2581-2592.
701

702   Schaap, M., Otjes, R.P., and Weijers, E.P., 2011. Illustrating the benefit of using hourly
703   monitoring data on secondary inorganic aerosol and its precursors for model evaluation. . Atmos.
704   Chem. Phys., 11, 11041-11053.
705

706   Seinfeld, J.H., and Pandis, S.N., 2006. Atmospheric Chemistry and Physics. John Wiley & Sons,
707   New York, 2nd edition.
708

709   Shi, Y., Chen, J., Hu, D., Wang, L., Yang, X., and Wang, X., 2014. Airborne submicron
710   particulate(PM1) pollution in Shanghai, China: Chemical variability, formation/dissociation of
711   associated semi-volatile components and the impacts on visibility. Science of the total
712   environment, 473, 199-206.
713

714   Trebs, I., Meixner, F.X., Slanina, J., Otjes, R., Jongejan, P., and Andreae, M.O., 2004. Real-time
715   measurements of ammonia, acidic trace gases and water-soluble inorganic aerosol species at a
716   rural site in the Amazon Basin. Atmos. Chem. Phys., 4, 967-987.
717

718   Trebs, I., Andreae, M.O., Elbert, W., Mayol-Bracero, O.L., Soto-Garcia, L.L., Rudich, Y.,
719   Falkovich, A.H., Maenhaut, W., Artaxo, P., Otjes, R., and Slania, J., 2008. Aerosol inorganic
720   composition at a tropical site: discrepancies between filter-based sampling and a semi-
721   continuous method. Aerosol Sci. Tech., 42, 255-269.
722

723   Twigg, M.M., Di Marco, C.F., Leeson, S., van Dijk, N., Jones, M.R., Leith, I.D., Morrison, E.,
724   Coyle, M., Proost, R., Peeters, A.N.M., Lemon, E., Frelink, T., Braban, C.F., Nemitz, E, and
725   Cape, J.N., 2015. Water soluble aerosols and gases at a UK background site-Part 1: Controls of
726   PM2.5 and PM10 aerosol composition. Atmos. Chem. Phys., 15, 8131-8145.
727

728   U.S. Environmental Protection Agency (U.S. EPA), 2011. Environmental Technology
729   Verification report: Applikon MARGA semi-continuous ambient air monitoring system. U.S.
730   EPA, Office of Research and Development. EPA/600/R11106VR.

731   van Os, M.J., Slanina, J., de Ligny, C.L., and Agterdenbos, J. 1984. Linear calibration in ion
732   chromatography by calculating total amounts of sample from measured conductivity data. Anal.
733   Chim. Acta, 156, 169-180.

734   Vayenas, D.V., Takahama, S., Davidson, C., Pandis, S.N., 2005. Simulation of the
735   thermodynamic and removal processes in the sulfate-ammonia-nitric acid system during winter:
736   Implication for PM2.5 control strategies. J. Geophys. Res., 110, DOI:10.1029/2004JD005038.
737

738   Weber, R.J., Orini, D., Daun, Y., Lee, Y-N., Klotz, P.J., and Brechtel, F., 2001. A Particle-into-
739   Liquid collector for rapid measurement of aerosol bulk chemical composition. Aerosol Sci.
740   Tech., 35, 718-727.
741

742   Weber, R., Orsini, D., Duan, Y., Baumann, K., Kiang, C.S., Chameides,W., Lee, Y.N., Brechtel,
743   F., Klotz, P., Jongejan, P., ten Brink, H., Slanina, J., Boring, C.B., Genfa, Z., Dasgupta, P.,
744   Hering, S., Stolzenburg, M., Dutcher, D.D., Edgerton, E., Hartsell, B., Solomon, P., and Tanner,
745   R., 2003. Intercomparison of near real time monitors of PM2.5 nitrate and sulfate at the U.S.
746   Environmental Protection Agency Atlanta Supersite. J. Geophy. Res., 108, 8421,
747   doi:10.1029/2001JD001220.
748

749   Wolff, V., Trebs, I., Ammann, C., Meixner, F.X. 2010. Aerodynamic gradient measurements of
750   the NH_3-HNO_3-NH_4NO_3 triad using a wet chemical instrument: an analysis of precision
751   requirements and flux errors. Atmos. Meas. Tech., 3, 187–208.
752

753   Wyers, G.P., Otjes, R.P., and Slanina J., 1993. A continuous-flow denuder for the measurement
754   of ambient concentrations and surface-exchange fluxes of ammonia. Atmos. Environ., 27, 2085-
755   2090.
756

757

Tables

759 Table 1. Method detection limits for chromatograms processed by MARGA tool and re-

760 integrated by Chromeleon.

	Chromeleon		MARGA tool	
	MDL(μg/m^3)	# of sample	MDL(μg/m^3)	# of sample
NH$_4^+$	0.02	78	0.04	78
NH$_3$	0.02	78	0.04	78
SO$_4^{2-}$	0.08	80	0.13	76
SO$_2$	0.05	80	0.08	76
NO$_3^-$	0.08	80	0.14	76
HNO$_3$	0.08	80	0.14	76

761

762

763

764

765

766

767

768

769

770

771

772

773

774

775

776

777 Table 2. Comparison between MARGA sample boxes 1 and 2 for particulate NO_3^-, SO_4^{2-} and

778 NH_4^+, gas phase HNO_3, SO_2 and NH_3 by orthogonal least squares regression. *N* is number of

779 observations, $C_{average}$ is average air concentration, $\sigma_{\Delta C}$ is the standard deviation of the orthogonal

780 least squares residuals (i.e., detection limit (DL)), $\sigma_{\Delta C}/C_{avg}$ is the precision estimate, C_{max} and

781 C_{min} are the maximum and minimum air concentrations, respectively. Percentage of observations

782 below the detection limit (DL) is also included.

|	Slope	Intercept	$\sigma_{\Delta C}$ $\mu g/m^3$	N	$C_{average}$ $\mu g/m^3$	C_{max} $\mu g/m^3$	C_{min} $\mu g/m^3$	$\sigma_{\Delta C}/C_{avg}$ %	<DL%
NH_4^+	0.98	0.01	0.02	616	0.52	2.20	0.10	4	0
NH_3	1.02	-0.03	0.03	614	0.33	1.62	0	9	5
SO_4^{2-}	0.99	0.01	0.05	602	1.41	4.39	0.17	4	0
SO_2	0.96	0.02	0.15	603	0.98	23.26	-0.01	15	27
NO_3^-	1.00	0.00	0.01	602	0.21	3.18	0	5	17
HNO_3	0.83	0.01	0.03	603	0.19	0.97	0	16	20

783

784

785   Table 3. Summary of concentrations ($\mu g/m^3$) of aerosol and precursor gases during and outside
786   of cold air mass periods.

	Cold Event			Non-Cold event		
	Average	Median	Max	Average	Median	Max
NH_3	0.12	0.09	0.29	0.35	0.24	1.62
HNO_3	0.35	0.30	0.82	0.17	0.13	0.97
SO_2	3.22	1.32	32.56	0.73	0.42	8.09
NH_4^+	0.99	0.88	2.20	0.48	0.45	1.21
NO_3^-	1.07	0.72	3.18	0.13	0.09	0.98
SO_4^{2-}	1.93	1.66	4.39	1.33	1.29	3.58
Temperature	4.54	5.00	13.9	12.88	12.20	29.40
RH	50	51	77	70	71	100

787

788

789

790   **Figures**
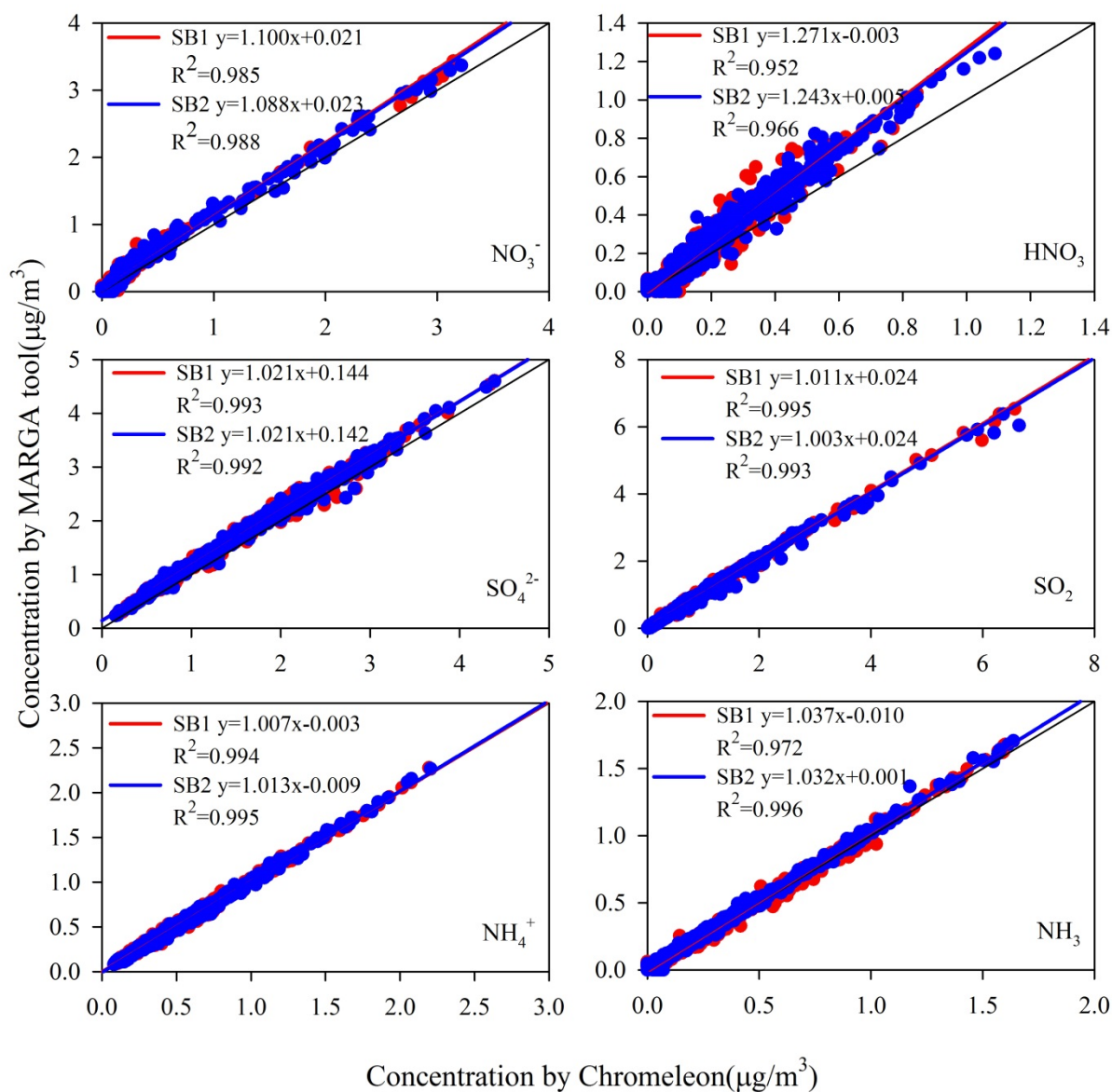
791

792   Figure 1. Comparison of concentrations of analytes monitored during fall of 2014 at Duke Forest
793   as reported by MARGA tool and Chromeleon. Data points with misintegration issues by
794   MARGA tool were excluded from this comparison. Data for individual sample boxes (SB1 and
795   SB2) are shown.

796

797

798

799
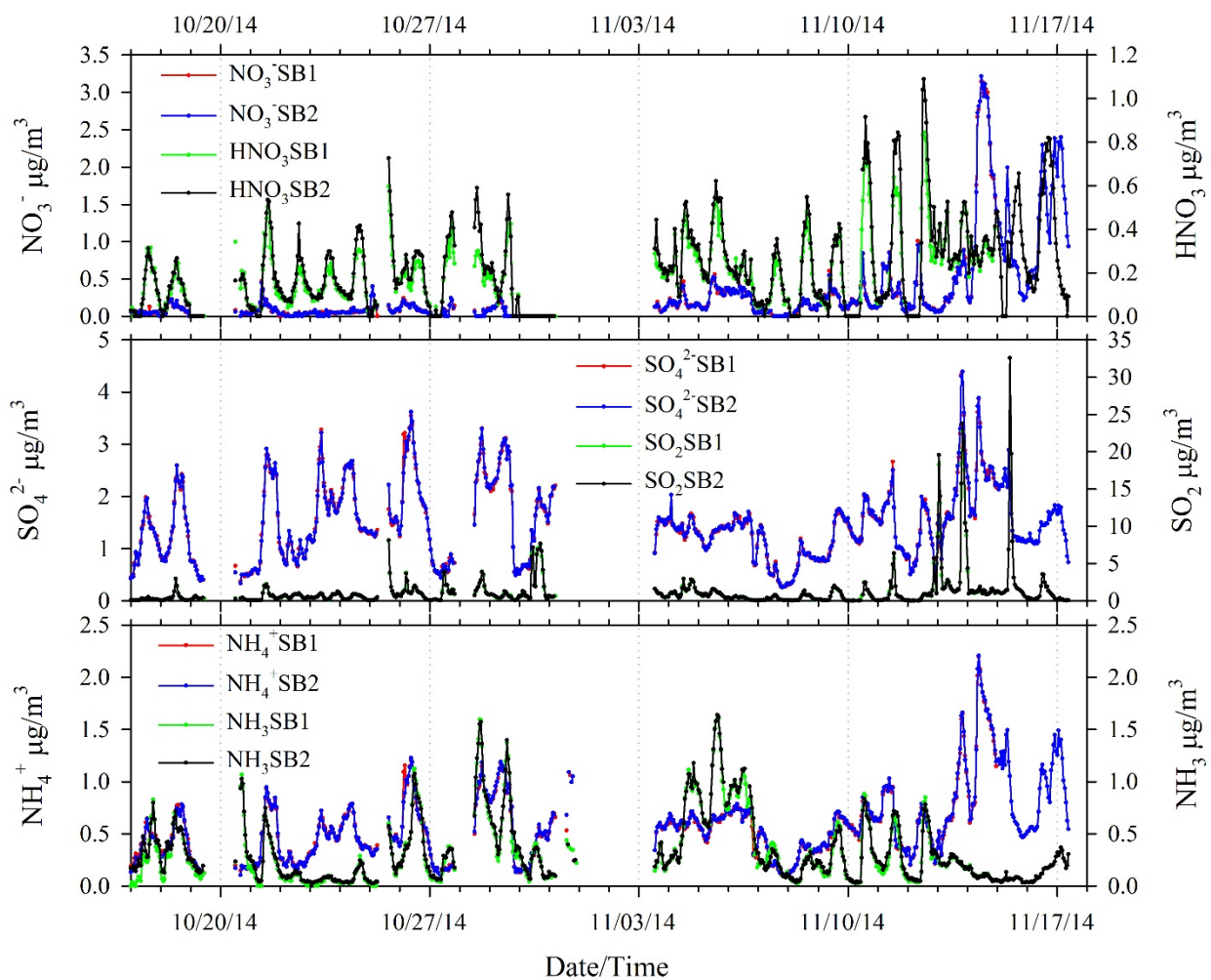
Figure 2. Time series of concentrations of particulate NO_3^-, SO_4^{2-} and NH_4^+, gas phase HNO_3,

801   SO_2 and NH_3 by collocated MARGA sample boxes 1 (SB1) and 2 (SB2).

802

803

804

805

806

807
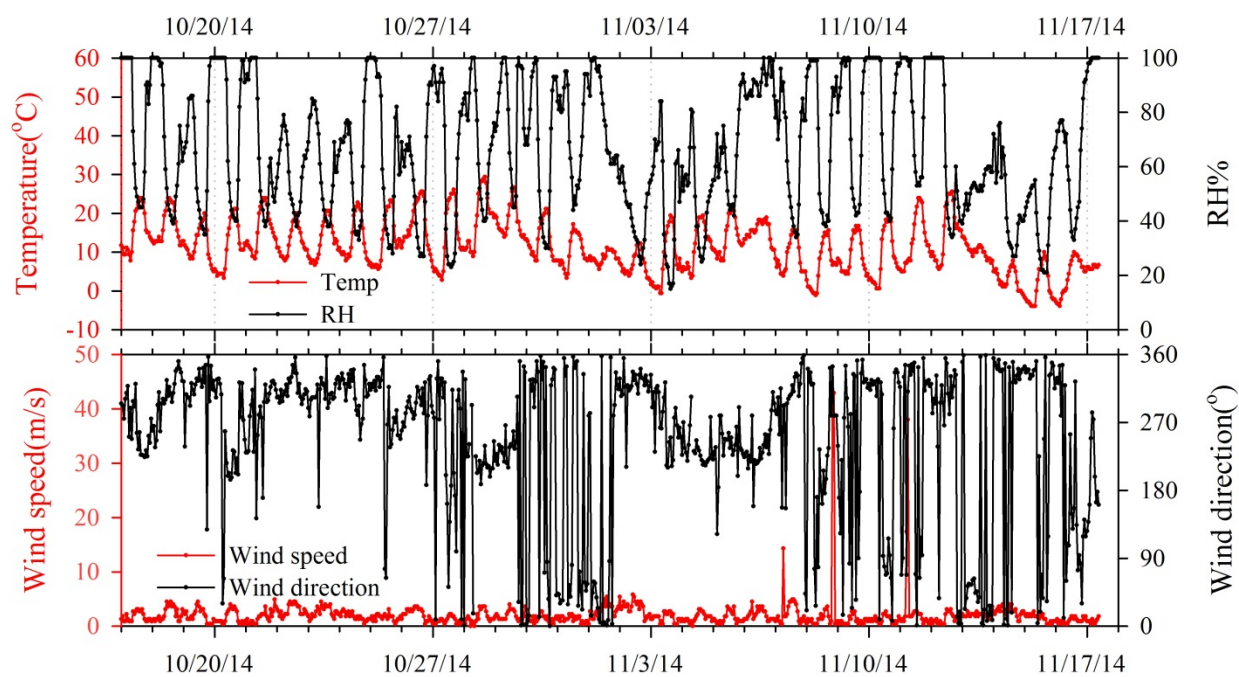
Figure 3. Hourly temperature, relative humidity, wind speed and wind direction during the fall
2014 field intensive.

808
809

810

811

812

813

814

815

816

817

818

819

820

821

822
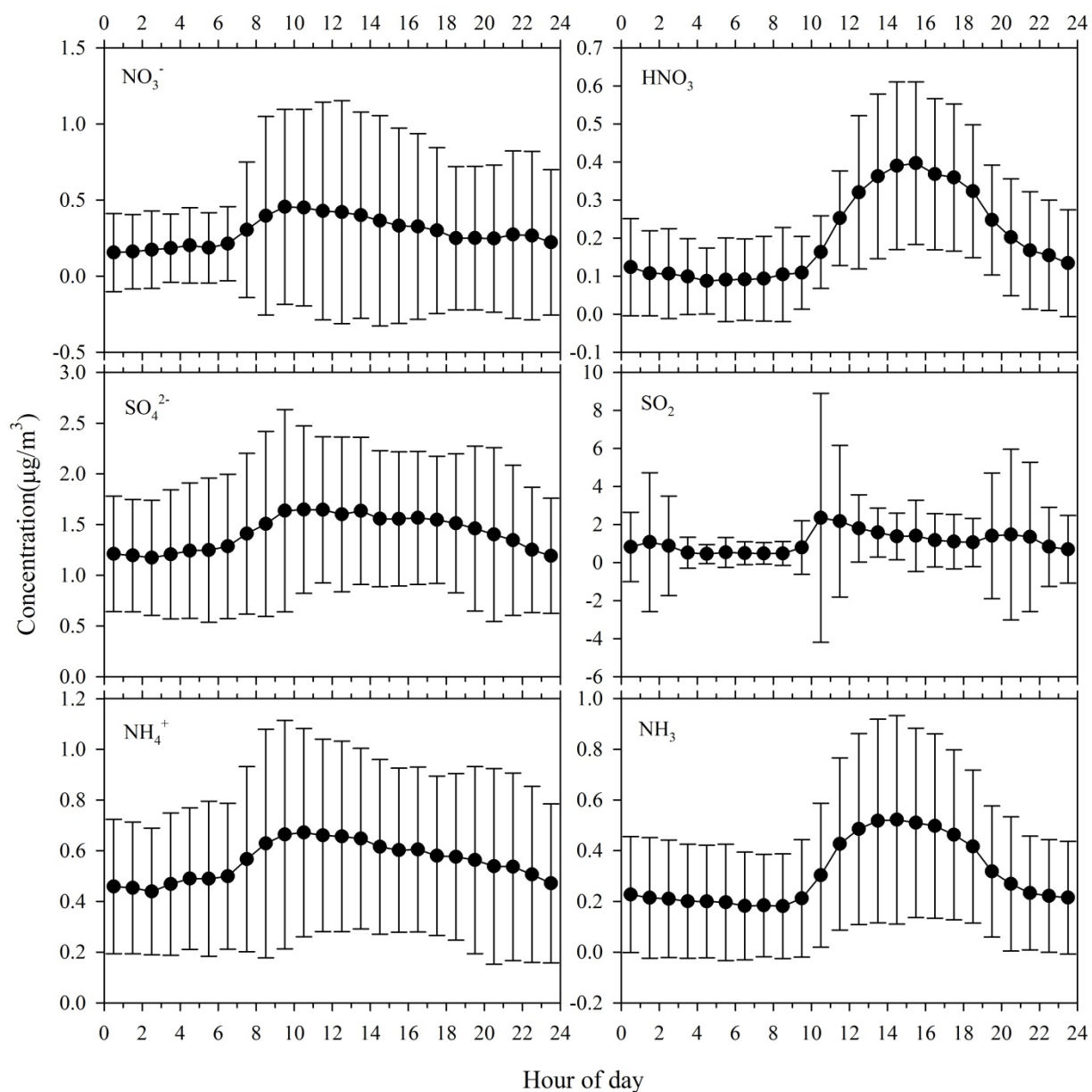
Figure 4. Diurnal profiles of particulate NO_3^-, SO_4^{2-} and NH_4^+, gas phase HNO_3, SO_2 and NH_3 during the fall 2014 field intensive. Data points represent average concentrations, while error bars represent 1 standard deviation.

826

827

828

829
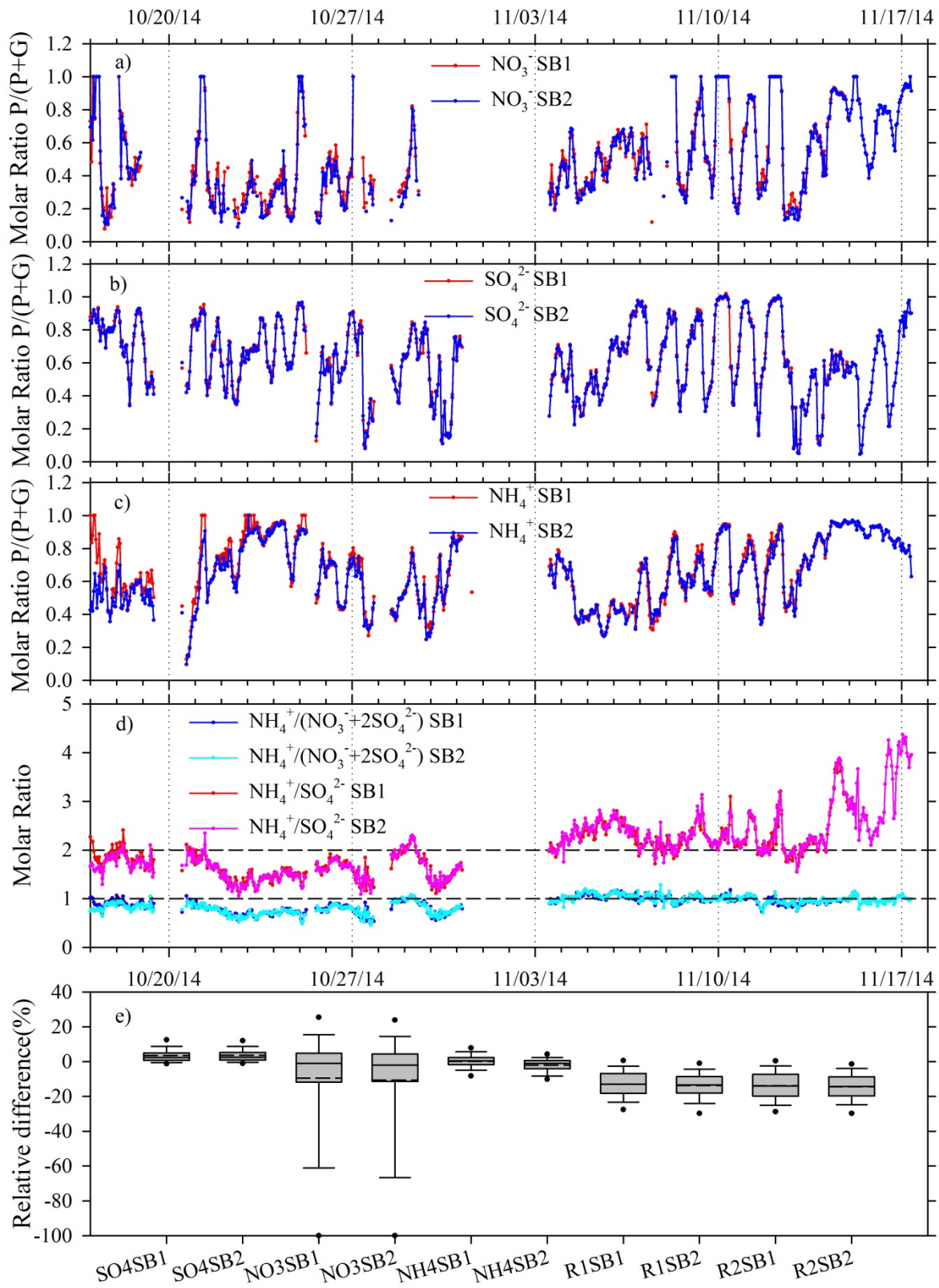
831   Figure 5. Partitioning molar ratios of a) NO_3^-, b) SO_4^{2-} and c) NH_4^+ in particle phase, calculated
832   as particle/(particle+gas); d) molar ratios (R1and R2) of particulate NO_3^-, SO_4^{2-} and NH_4^+ to
833   determine particle neutralization state and acidity; e) relative difference of partitioning molar
834   ratios of NO_3^-, SO_4^{2-} and NH_4^+ in particle phase as well as particle neutralization state indicators
835   R1 and R2 by Chromeleon and MARGA tool. Negative values indicate a lower ratio calculated
836   by the MARGA tool (i.e., positive bias in concentrations calculated by MARGA tool). Solid and
837   dash lines inside box represent median and mean, respectively. Top and bottom box represent
838   75th and 25th percentiles. Whiskers represent 90th and 10th percentiles. Dots represent 95th and 5th
839   percentiles. SB1 and SB2 indicate collocated MARGA sample boxes 1 and 2, respectively.
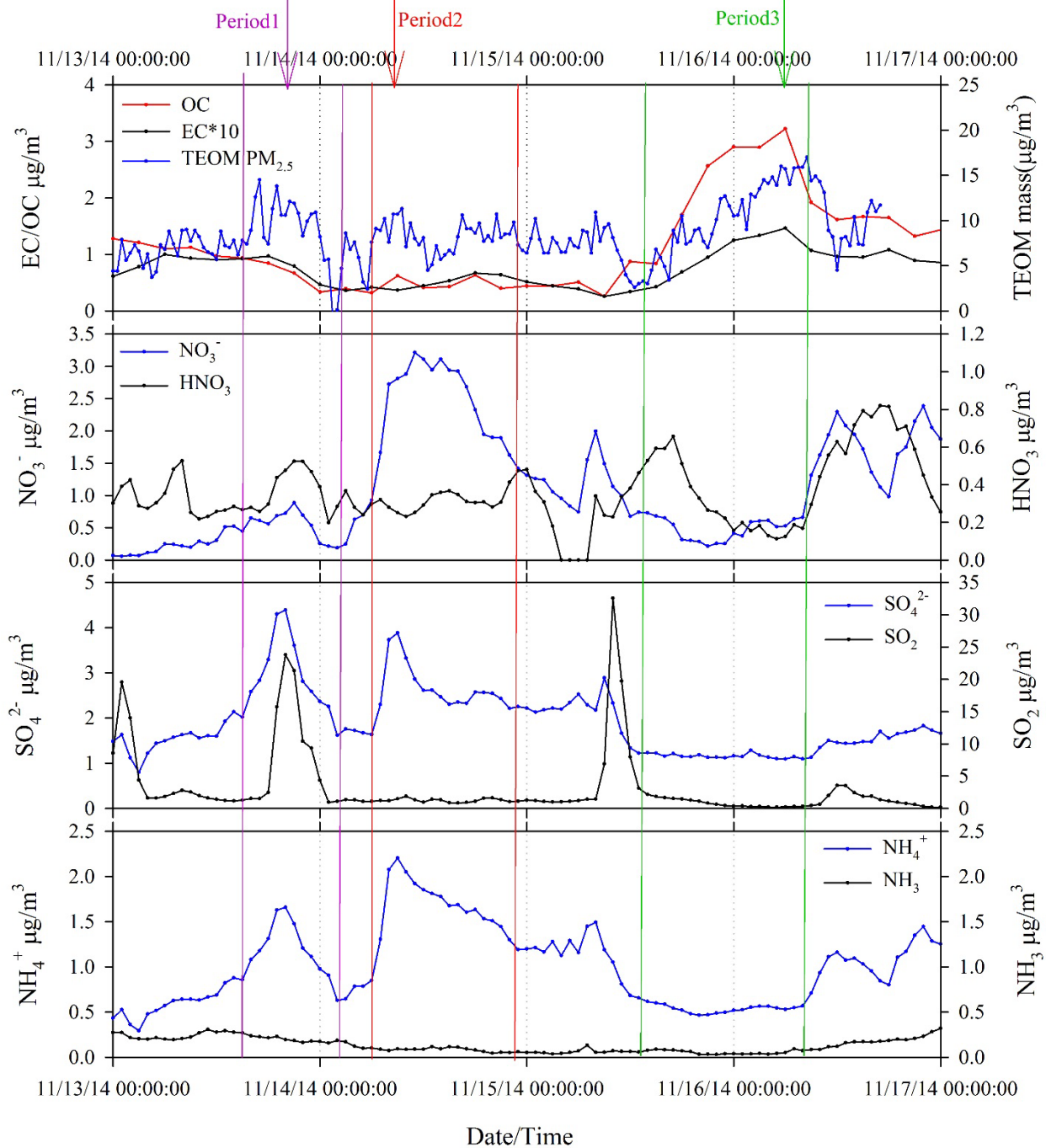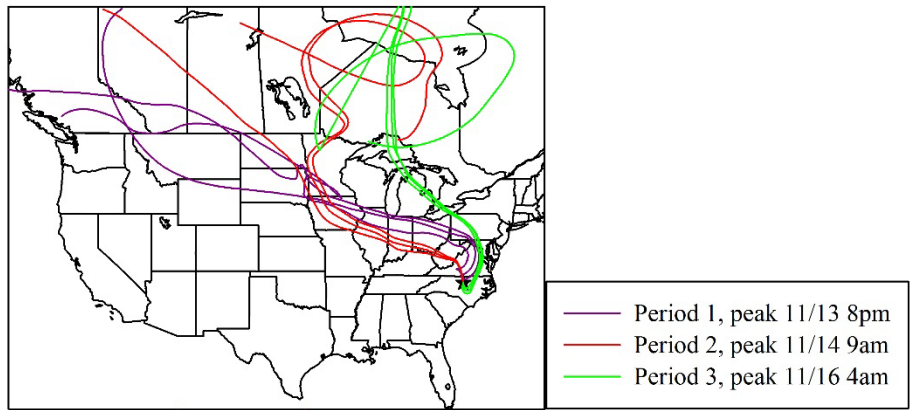
841   Figure 6. High concentration periods observed during mid-November 2014. Period 1: highest

842   SO_4^{2-}; Period 2: highest NH_4^+ and NO_3^-; Period 3: highest OC. Corresponding back trajectories

843   (arrival at 500AGL, backwards for 168hrs) of individual period peaks (±2hrs) are also presented.

844

845

846

847

848

849

850

851

852

853

854

855

856

857

858

859

860

861

862

863

864